(Received 17 October 2025, Accepted 27 January 2026, Scheduled 27 February 2026)

Flexible Circular Ring Slot Antenna with AMC Structure for Wearable Applications

Said Abushamleh*

Indiana Institute of Technology, Indiana, USA

ABSTRACT: A flexible semicircular ring slot antenna with an artificial magnetic conductor (AMC) structure for wireless body area network application is proposed in this paper. The AMC structure is an array of double split ring resonator (DSRR) unit cells. According to the analysis of the DSRR unit cell, the volume of the AMC element is miniaturized for applications such as wearable technology. The measured impedance bandwidth of the proposed antenna is observed to be 2.34–2.61 GHz, which covers the 2.4 GHz Industrial Scientific Medical (ISM) band. The simulated half-power beamwidths are 81.1° and 70.1° in the E-plane and H-plane, respectively, and the front-to-back ratios are 17.51 dB in both the E-plane and H-plane. The calculated specific absorption rates (SARs) taken over the volume containing a mass of 1 g of tissue (U.S. standard) and 10 g of tissue (E.U. standard) are both less than the limitations. In conclusion, it is proper to use the proposed flexible antenna in wearable applications.

1. INTRODUCTION

Wireless body area networks (WBANs) are important for enabling continuous, unobtrusive health monitoring, facilitating remote healthcare, and improving quality of life for patients, i.e., allowing them to move freely while data is collected. Consequently, wearable antennas have become integral to body-centric wireless systems.

The design of wearable antennas, however, faces significant challenges, including performance degradation due to human body proximity, mechanical deformation under bending or stretching, and compliance with electromagnetic safety standards such as SAR. Despite these constraints, wearable antennas provide advantages such as enhanced mobility, hands-free operation, and energy-efficient communication. Emerging applications include real-time health monitoring, secure military communications, sports performance tracking, and integration into smart textiles for internet of things (IoT) and augmented reality systems, positioning wearable antennas as a key enabler of next-generation pervasive networks.

The importance of researching wearable antennas is clearly visible in the widespread use of WBAN systems, such as antenna-integrated garments [1], bags [2], glasses [3], and smart watches [4]. A symmetrically crumpled antenna is studied in [5], and an irregularly crumpled antenna was studied in [6]. It is important to recall the major design aspects during the design of wearable antennas: comfort level and specific absorption rate (SAR).

To consider the comfort level, flexible materials can be used, so they can be bent when a human moves. Moreover, the potential harm to the human body from the wearable antenna should be considered because the antenna is placed close to the human body. The SAR values should satisfy the limitation defined by the U.S. or E.U. standards for SAR.

Antennas with low SAR values are proposed in [7] and [8]. However, the use of vias may affect the comfort level. Another method to reduce the SAR value is to use an electromagnetic bandgap (EBG) or artificial magnetic conductor (AMC) structure that has a zero reflect phase [9–14].

A miniaturized slotted Jerusalem Cross (JC) AMC is proposed in [9]. An inkjet-printed antenna on paper is proposed in [10], and a paper-based antenna is likely to be damaged. EBG is printed on latex and polydimethylsiloxane substrates in [11] and [12], respectively. However, the complexity of these structures is going to affect the comfort level.

In this paper, a double split-ring resonator is used to design the AMC structure that will be printed on a flexible, bendable, and comfortable substrate. The new AMC structure is simple as vias are not involved in the design of the structure. The antenna is easy to fabricate and achieves the design requirement. Finally, a low SAR value is presented and investigated.

2. ANTENNA DESIGN

2.1. Antenna Structure

Figure 1(a) illustrates the configuration of the wearable circular ring slot antenna, comprising a substrate layer and a copper layer. The used substrate layer is a flexible Rogers RO3006. The substrate's relative permittivity is 6.5, and its loss tangent is 0.002.

The substrate layer exhibits a volume of $W \times L \times 1.28\,\text{mm}^3$. The conductive layer is composed of flexible annealed copper (electrical conductivity $\sigma = 5.8\text{e}7\,\text{S/m}$) with a thickness of 0.035 mm. In this layer, a ground structure is incorporated, featuring a semicircular slot, with a radius designated as R_2,

* Corresponding author: Said A. Abushamleh (saabushamleh@indianatech.edu).

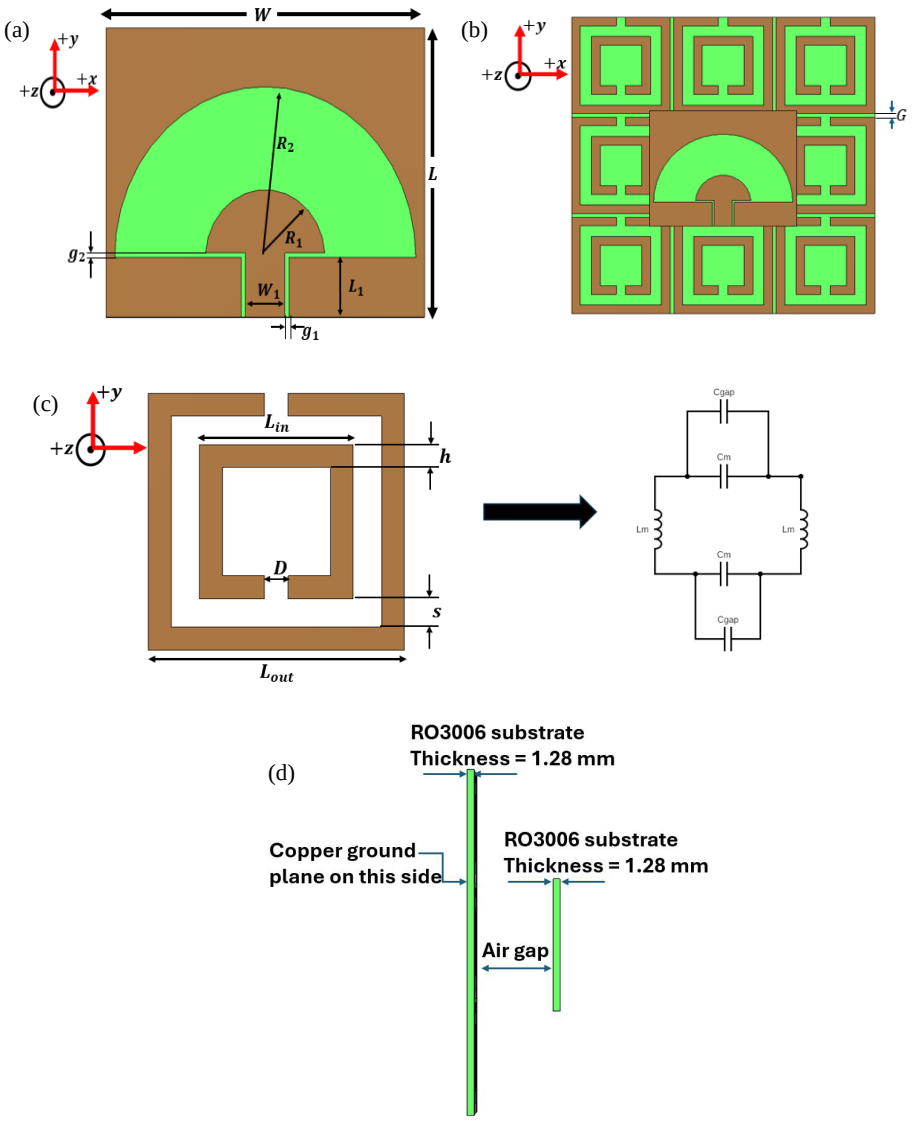

FIGURE 1. Fabricated antenna. (a) Wearable circular ring slot antenna. (b) Antenna with AMC structure. (c) AMC unit cell and its equivalent circuit model. (d) Side view.

and matching the dimensions of the dielectric substrate. The feeding mechanism consists of a semicircular element with a radius of R_1, centered precisely at the midpoint of the slot in the ground. The antenna is energized through a coplanar waveguide (CPW), exhibiting a characteristic impedance of 50 Ω.

The proposed antenna design exhibits primary radiation beams directed along the positive and negative z-axes. Consequently, individuals in proximity to the antenna will experience significant radiation exposure. To mitigate this concern, an antenna with artificial magnetic conductor (AMC) structure is illustrated in Fig. 1(b). A 3×3 DSRR array is positioned beneath the antenna, utilizing the same materials as the antenna itself. The DSRR unit cell and its equivalent circuit model are shown in Fig. 1(c). A side view of the antenna and AMC structure is shown in Fig. 1(d). The optimized parameters are specified as follows: $W = 65.6\,\text{mm}$, $L = 65.6\,\text{mm}$, $R_1 = 5.9\,\text{mm}$, $R_2 = 14.9\,\text{mm}$, $W_1 = 3.95\,\text{mm}$, $L_1 = 5.2\,\text{mm}$, $g_1 = 0.4\,\text{mm}$, $g_2 = 3.6\,\text{mm}$, $G = 0.8\,\text{mm}$, $L_{in} = 12.8\,\text{mm}$, $L_{out} = 21.3\,\text{mm}$, $D = 2$, $h = 1.9\,\text{mm}$, and $s = 2.4\,\text{mm}$.

2.2. Design of the AMC Structure

The DSRR unit cell is compared to the rectangular patch unit cell (without vias). For wearable applications, the vias in the rectangular mushroom AMC can impact comfort and complicate the manufacturing process. The equivalent circuit model of the rectangular patch that does not include vias is investigated in [14]. The DSRR circuit model is investigated in [15].

The DSRR functions as a resonant cavity, which can be effectively modeled using an LC circuit framework. When a magnetic field H is applied perpendicular to the plane of the two split rings, it facilitates the formation of capacitive gaps C_{gap} at each ring's opening. The interaction between these two metallic rings occurs through a mutual capacitance. Furthermore, each ring can be conceptualized as a solenoid, characterized by an inductance L_m. The region between the two rings is represented by a capacitance C_m. The corresponding electrical circuit is illustrated in Fig. 1(c).

Figure 2 shows the effect of R_1 on the antenna's S_{11}. Table 1 summarizes its impact on matching at 2.45 GHz and on

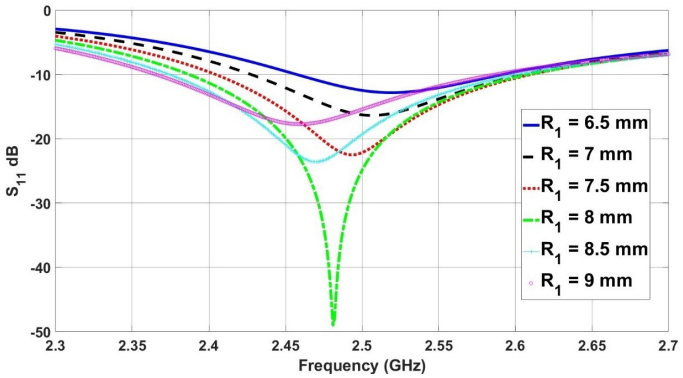

FIGURE 2. The effect of R_1 on impedance matching.

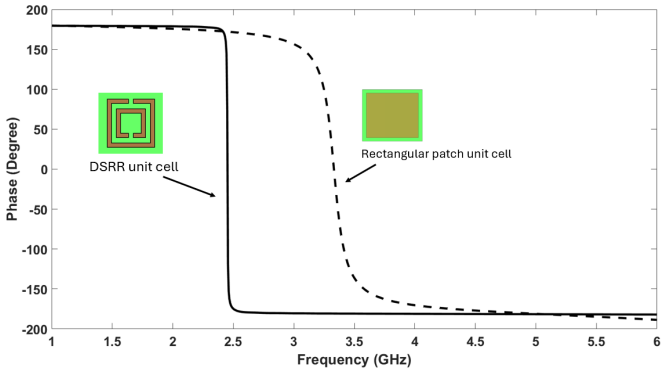

FIGURE 3. Reflect phase of the rectangular patch and DSRR.

TABLE 1. R_1's impact on matching at 2.45 GHz and on bandwidth.

R_1 (mm)	Matching value in dB at 2.45 GHz	Bandwidth (GHz)
6.5	−9.51	Range: 2.457–2.592 BW = 0.135
7.0	−12.1	Range: 2.427–2.606 BW = 0.179
7.5	−15.7	Range: 2.404–2.610 BW = 0.206
8.0	−19.9	Range: 2.387–2.609 BW = 0.222
8.5	−20.9	Range: 2.374–2.602 BW = 0.228
9.0	−17.6	Range: 2.365–2.588 BW = 0.223

TABLE 2. R_2's impact on matching at 2.45 GHz and on bandwidth.

R_2 (mm)	Matching value in dB at 2.45 GHz	Bandwidth (GHz)
17.9	−4.62 (No matching)	-
18.4	−7.64 (No matching)	-
18.9	−15.67	Range: 2.403–2.613 BW = 0.21
19.4	−14.02	Range: 2.318–2.500 BW = 0.182
19.9	−5.64 (no matching)	-

bandwidth. R_2 is fixed at 18.9 mm. All other parameters remain unchanged. Similarly, Table 2 summarizes the effect of R_2 on matching at 2.45 GHz and on bandwidth. R_1 is fixed at 7.5 mm. All other parameters remain unchanged. After adding the AMC structure, R_1 was set to 5.9 mm and R_2 to 14.9 mm.

The inductance L_m of each ring is represented by the following equation:

$$L_m = \frac{\mu_0 s}{h}\left[L_{out} + L_{in}\right] \tag{1}$$

The capacity C_{gap} of the slot ring is determined by the following equation:

$$C_{gap} = \frac{\varepsilon_0 \varepsilon_r t_c}{D} \tag{2}$$

The capacity C_m between the two rings is expressed as follows:

$$C_m = \frac{A\varepsilon_0 \varepsilon_r h\left(2L_{out} + 2L_{in} - D\right)}{2s} \tag{3}$$

where L_{out} and L_{in} are the lengths of the outer and inner square rings, respectively; h is the width of the strip of the metal ring; s is the space between the two rings; D is the gap in each ring. Finally, A is a balance or equilibrium constant given by:

$$A = \frac{c^2}{4\pi^2 (L_{out} + L_{in})^2 f_0^2 \varepsilon_r} \tag{4}$$

where $c = 3 \times 10^8$ m/s is the speed of light.

The resonant frequency f_0 can be determined based on the geometric parameters such as:

$$f_0 = \frac{1}{2\pi\sqrt{L_m(C_m + C_{gap})}} \tag{5}$$

If we increase C_{gap} and C_m, we can decrease the frequency of operation. Fig. 3 illustrates the comparison of the reflection phase characteristics between the rectangular patch (AMC) structure and DSRR structure, both featuring identical unit sizes. Notably, the zero-reflection phase frequency for the rectangular patch AMC is identified at 3.47 GHz, whereas the corresponding frequency for the DSRR AMC is determined to be 2.47 GHz. This analysis indicates that, given the same resonant frequency, the DSRR configuration achieves a reduced physical volume in the design of the AMC structure.

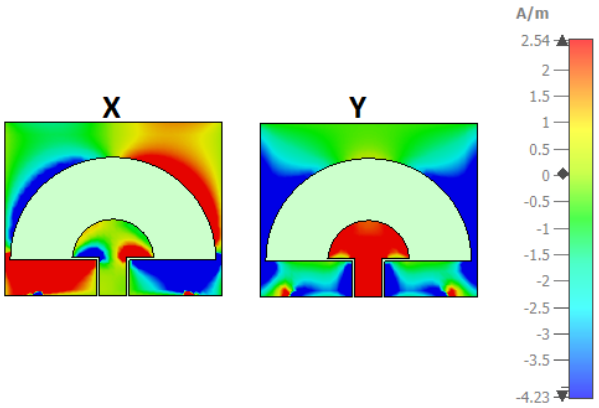

FIGURE 4. Surface current distribution for the proposed antenna at $f = 2.45$ GHz in x- and y-components.

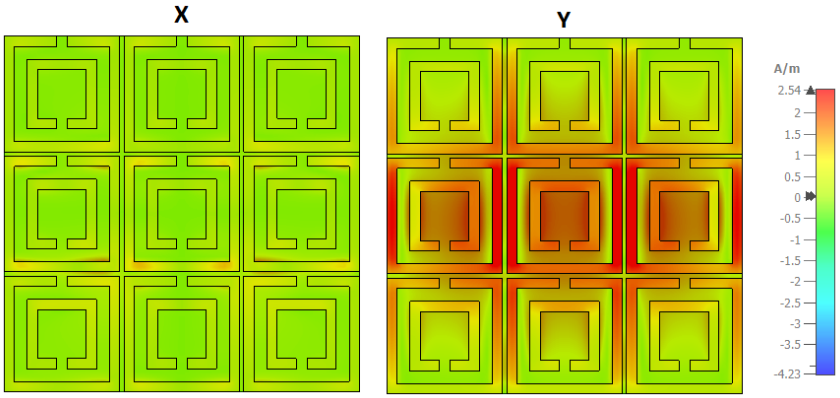

FIGURE 5. Surface current distribution for the proposed AMC structure at $f = 2.45$ GHz in x- and y-components.

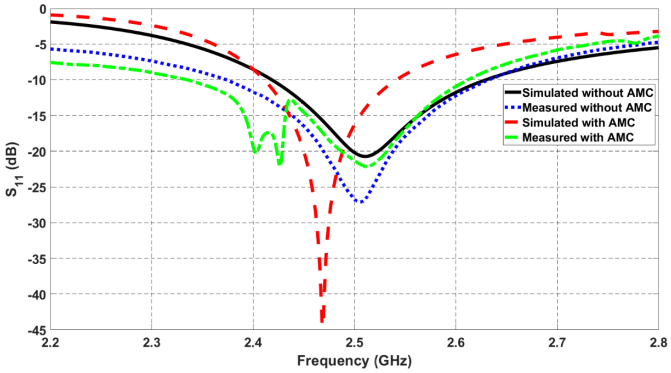

FIGURE 6. Simulated and measured S_{11} of the proposed antenna with/without AMC.

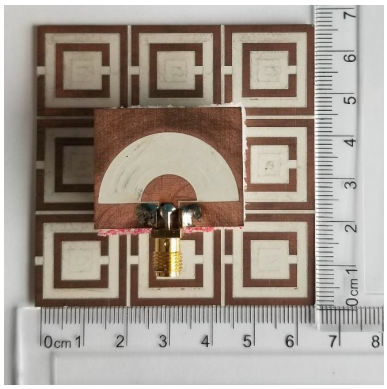

FIGURE 7. Antenna prototype with the AMC structure.

The current distribution of the proposed antenna at 2.45 GHz is illustrated in Fig. 4. It is observed that the surface current exhibits a concentration around the feedline of the coplanar waveguide (CPW) and the ring slot, displaying a symmetrical distribution along the y-axis. The horizontal components of the current are equal and opposite, effectively canceling each other out, while the vertical components are equal and aligned, thereby reinforcing one another; consequently, the antenna operates in a y-polarized mode.

Resonance is detected within each unit cell. Resonance is obvious by analyzing the current distribution on the AMC structure as shown in Fig. 5. The AMC structure is placed under the radiation element. The currents exhibit horizontal offsets while being enhanced in the vertical plane. This configuration facilitates the reflection of radiation in the negative z-direction, ensuring that it does not adversely affect the surrounding human body.

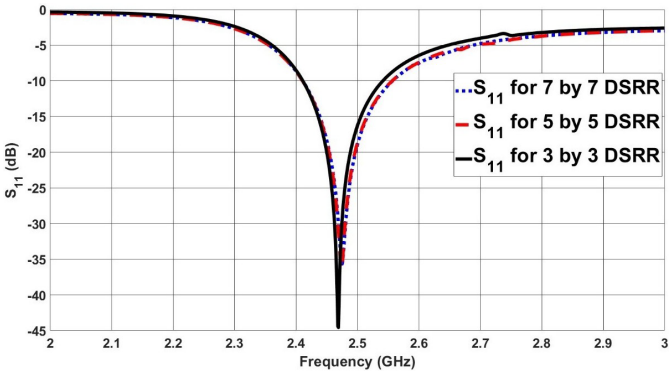

FIGURE 8. S_{11} for three AMC configurations using DSRR unit cells: 3×3, 5×5, and 7×7 arrays.

3. SIMULATED AND MEASURED RESULTS

3.1. S_{11} Parameter

Figure 6 presents the reflection coefficients for the antenna both with and without the artificial magnetic conductor (AMC) structure. Notably, the center frequency of the antenna incorporating AMC exhibits a shift towards lower frequencies compared to its counterpart without AMC. The measured bandwidth for the S_{11} parameter ≤ -10 dB for the AMC-integrated antenna is determined to span from 2.34 to 2.61 GHz. This measured bandwidth is slightly broader than the simulated prediction, which ranges from 2.40 to 2.54 GHz. Both AMC-based antenna configurations (simulated and measured) effectively encompass the 2.4 GHz Industrial Scientific Medical (ISM) band at 2.40–2.4835 GHz, as illustrated in Fig. 6. The fabricated prototype is shown in Fig. 7. A foam layer is used between the radiating element and the AMC structure, and its dielectric properties, flexibility, and durability are verified to ensure stable antenna performance and suitability for wearable

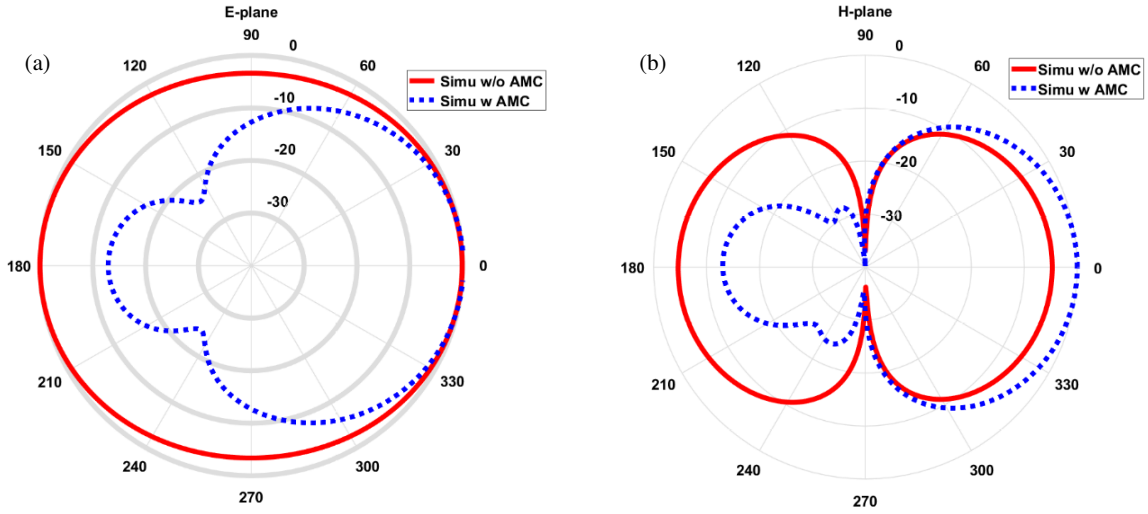

FIGURE 9. Simulated and measured radiation patterns of the proposed antenna at 2.45 GHz. (a) E-plane, (b) H-plane.

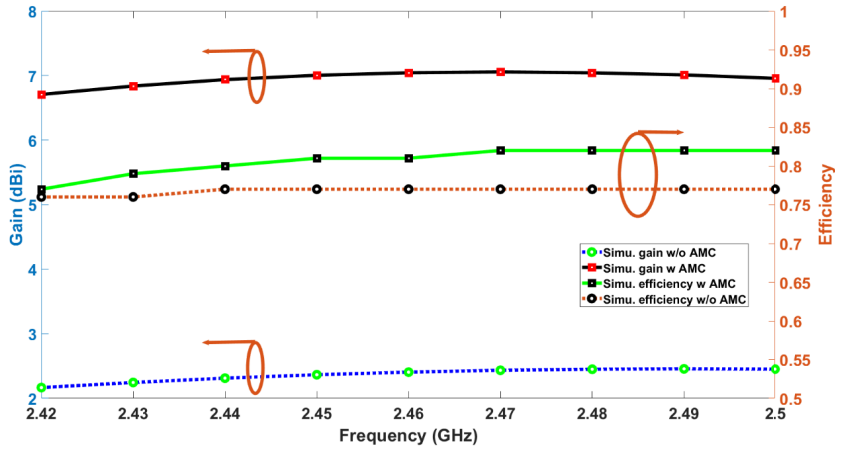

FIGURE 10. Gain and efficiency of the proposed antenna.

applications. S_{11} is simulated in Fig. 8 for three AMC configurations using DSRR unit cells: 3×3, 5×5, and 7×7 arrays. All configurations exhibited similar performance. Each structure achieved approximately -20 dB for S_{11} at 2.45 GHz. Based on these results, the 3×3 DSRR AMC configuration was selected.

3.2. Radiation Patterns

The radiation patterns in the xz plane (E-plane) at a frequency of 2.45 GHz are illustrated in Fig. 9(a). Observations reveal that for the antenna without an AMC, an omnidirectional radiation pattern is evident, with a slight compression occurring in the x-direction. Conversely, Fig. 9(b) depicts the radiation pattern in the yz plane (H-plane), characterized by a figure-eight shape, where peak radiation is directed along the z-axis, while a null point is present in the y-axis. These radiation characteristics can also be interpreted through the in-phase (equal and aligned) current vertical components as depicted in Fig. 4, thereby reinforcing one another. Consequently, the antenna operates in a y-polarized mode.

In the case of the AMC-integrated antenna, unidirectional radiation patterns are obvious in both the E-plane and H-plane. The simulated half-power beamwidths are recorded at 81.1° and 70.1° in the E-plane and H-plane, respectively. The front-to-back ratios (FBRs) measure 17.51 dB in both the H-plane and E-plane. The data illustrates that the incorporation of AMC effectively reduces electromagnetic radiation in the negative z-direction.

3.3. Antenna Gain and Efficiency

The gain and efficiency characteristics of the antenna are depicted in Fig. 10. The antenna incorporating an Artificial Magnetic Conductor (AMC) demonstrates a notable enhancement in measured gain compared to its counterpart without AMC. The proposed antenna with AMC structure achieves a peak gain of 7.1 dBi within the ISM band. Furthermore, the efficiency of the antenna without the proposed AMC ground ranges from 75% to 80%. However, the presence of the AMC results in an improvement, i.e., elevating the efficiency to exceed 80%.

3.4. Effects of the Human Body

To assess the impact of the human body on antenna performance, the antenna was positioned on various body parts and subjected to slight bending. Fig. 11(a) illustrates the experi-

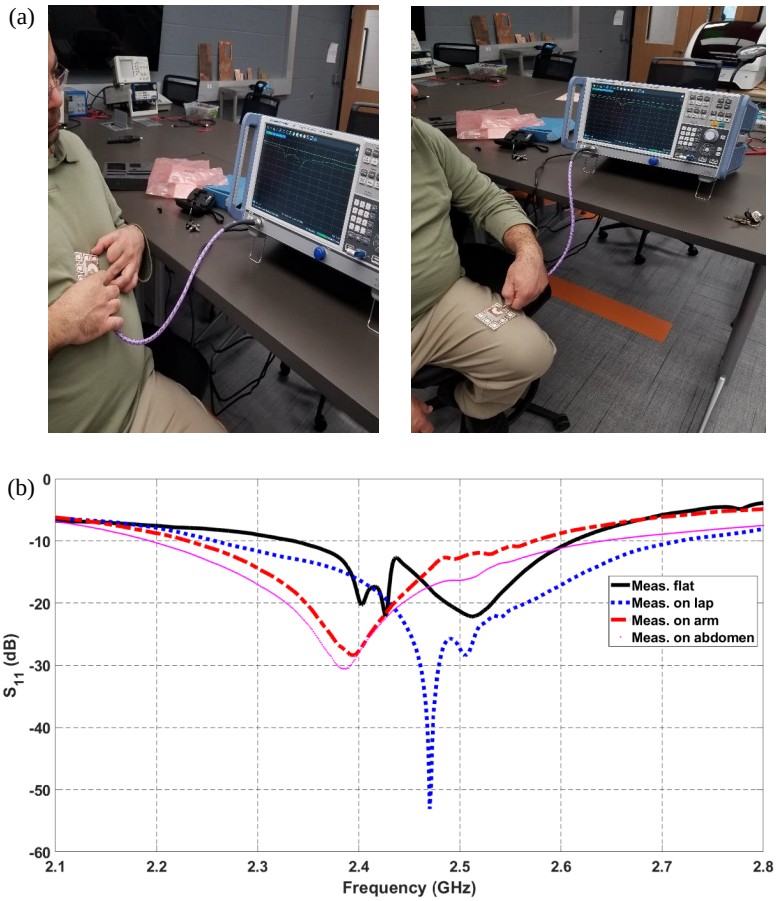

FIGURE 11. (a) Proposed antenna on human body. (b) Curves of measured S_{11} curves of the proposed antenna placed on the human body.

TABLE 3. Material properties of the human body model.

	Skin	Fat	Muscle	Bone
ε_r	37.95	5.27	52.67	18.49
Density (kg/m^3)	1001	900	1006	1008
Thickness (mm)	2	5	20	13
σ (S/m)	1.49	0.11	1.77	0.82

TABLE 4. SAR values of the antennas at 2.45 GHz (unit: W/kg).

	Max value	Without AMC	With AMC
1 g standard (U.S.)	1.6	7.11	0.66
10 g standard (EUR)	2.0	3.87	0.31

mental configuration of the proposed antenna both in free space and when being positioned on the arm, lap, and abdomen. The S_{11} reflection coefficient curves for the proposed antenna under these different scenarios were recorded and are presented in Fig. 11(b). Notably, the S_{11} curves exhibit only marginal variations, while the bandwidths corresponding to $S_{11} \leq -10$ dB satisfy the WBAN spectrum across all tested conditions.

3.5. SAR Evaluation

To assess the impact of the proposed antenna on the human body, specific absorption rate (SAR) values were simulated and compared for antennas with and without the presence of an artificial magnetic conductor (AMC). The human body was represented within the Computer Simulation Technology (CST) Microwave Studio software, utilizing the electromagnetic parameters outlined in Table 3 [16]. The human body model dimensions are $100 \times 100 \times 40\,\text{mm}^3$.

Figure 12 illustrates the SAR value for the antenna without AMC. The SAR was calculated based on both 1 g and 10 g mass standards. Analysis reveals that the zone with peak radiation occurs at the antenna's center. The maximum SAR value for the 1 g standard is determined to be 7.11 W/kg, exceeding the U.S. limit of 1.6 W/kg. For the 10 g standard, the maximum SAR value is recorded at 3.87 W/kg, which also surpasses the European threshold of 2.0 W/kg.

Figure 13 depicts the scenario following the integration of AMC into the antenna design, showing that the radiation disperses among the unit cells in two distinct directions: to the left and to the right. This modification leads to a substantial reduction of radiation in the central region of the antenna, demonstrating the AMC's effectiveness in minimizing SAR values. The maximum SAR value corresponding to the 1 g standard is now measured at 0.66 W/kg, signifying a reduction of 91%

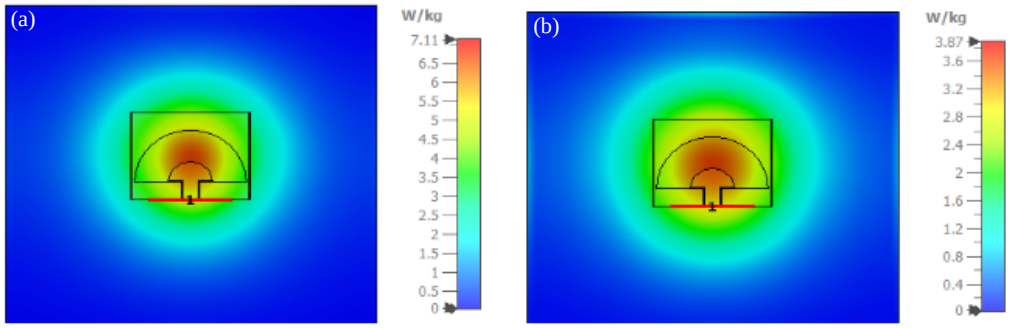

FIGURE 12. Simulated SAR (at 2.45 GHz) of the proposed antenna without AMC. (a) 1 g standard, (b) 10 g standard.

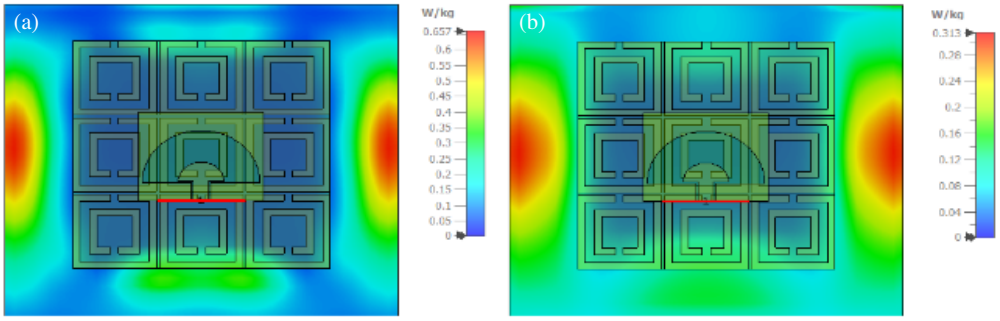

FIGURE 13. Simulated SAR (at 2.45 GHz) of the proposed antenna with AMC. (a) 1 g standard, (b) 10 g standard.

TABLE 5. Comparison of the proposed antenna with some references.

Ref.	Freq./GHz	Bandwidth/%	Gain/dBi	FBR/dB	Reflect/plane	Volume/mm × mm × mm
[4]	2.4	< 10	6.3	-	HIS	$38 \times 38 \times 3$
[7]	2.45/5.8	1.2/2.0	1.77/3.14	-	-	986(area) $\times$ 1.58
[8]	2.45	4.8	4.2	-	-	3326(area) $\times$ 3.7
[9]	2.45	18	4.8	8	AMC	$45 \times 30 \times$ N/A
[11]	2.4	1.88	4.12	> 12	AMC	$50 \times 50 \times 9.5$
[12]	2.4	11.3	5.2	12	-	$50 \times 50 \times 5.5$
[13]	2.45/5.8	-/15.4	4	> 12	AMC	$100 \times 100 \times 3$
[17]	2.45	5.3	5.37	-	AMC	$20 \times 30 \times 3$
[18]	5.8	3.6	4.1	-	Shorting Pins	$50 \times 50 \times 3$
[19]	2.45	2.4	4.36	-	EBG	$50 \times 50 \times 3$
Proposed structure	2.45	11	7.1	17.51	AMC	$65.6 \times 65.6 \times 2.56$

compared to the configuration without AMC. For the 10 g standard, the maximum SAR value is mere 0.31 W/kg, which is 92% lower than the counterpart without AMC.

A comparative analysis of these calculations relative to established limits is detailed in Table 4, confirming that the proposed antenna complies with the SAR regulations set forth by both U.S. and European standards.

4. CONCLUSION

In conclusion, this paper presents a wearable antenna featuring an AMC structure specifically designed for WBAN applications. A detailed comparison, illustrated in Table 5, highlights the superior bandwidth of our proposed antenna relative to those documented in previous studies. Notably, the peak gain and front-to-back ratio (FBR) of our antenna surpass those of the counterparts listed in Table 5.

The investigation into the AMC unit cells, utilizing the equivalent circuit model and current distribution analysis, reveals promising results. Measured S_{11} values demonstrate excellent impedance matching within the ISM band. Furthermore, the radiation patterns, antenna gain, efficiency, and specific absorption rate (SAR) values confirm that our design adheres to the SAR regulations established by both U.S. and European standards. Consequently, the proposed antenna shows great potential for integration into wearable technology.

REFERENCES

[1] Vallozzi, L., P. Van Torre, C. Hertleer, H. Rogier, M. Moeneclaey, and J. Verhaevert, "Wireless communication for firefighters using dual-polarized textile antennas integrated in their garment," *IEEE Transactions on Antennas and Propagation*, Vol. 58, No. 4, 1357–1368, Apr. 2010.

[2] Monti, G., L. Corchia, E. De Benedetto, and L. Tarricone, "Wearable logo-antenna for GPS-GSM-based tracking systems," *IET Microwaves, Antennas & Propagation*, Vol. 10, No. 12, 1332–1338, 2016.

[3] Hong, S., S. H. Kang, Y. Kim, and C. W. Jung, "Transparent and flexible antenna for wearable glasses applications," *IEEE Transactions on Antennas and Propagation*, Vol. 64, No. 7, 2797–2804, Jul. 2016.

[4] Chen, Y.-S. and T.-Y. Ku, "A low-profile wearable antenna using a miniature high impedance surface for smartwatch applications," *IEEE Antennas and Wireless Propagation Letters*, Vol. 15, 1144–1147, 2016.

[5] Shakhirul, M. S., M. Jusoh, A. Sahadah, C. M. Nor, and H. A. Rahim, "Embroidered wearable textile antenna on bending and wet performances for UWB reception," *Microwave and Optical Technology Letters*, Vol. 56, No. 9, 2158–2163, 2014.

[6] Hu, B., G.-P. Gao, L.-L. He, X.-D. Cong, and J.-N. Zhao, "Bending and on-arm effects on a wearable antenna for 2.45 GHz body area network," *IEEE Antennas and Wireless Propagation Letters*, Vol. 15, 378–381, 2016.

[7] Zhu, X.-Q., Y.-X. Guo, and W. Wu, "A compact dual-band antenna for wireless body-area network applications," *IEEE Antennas and Wireless Propagation Letters*, Vol. 15, 98–101, 2016.

[8] Agneessens, S., S. Lemey, T. Vervust, and H. Rogier, "Wearable, small, and robust: The circular quarter-mode textile antenna," *IEEE Antennas and Wireless Propagation Letters*, Vol. 14, 1482–1485, 2015.

[9] Raad, H. R., A. I. Abbosh, H. M. Al-Rizzo, and D. G. Rucker, "Flexible and compact AMC based antenna for telemedicine applications," *IEEE Transactions on Antennas and Propagation*, Vol. 61, No. 2, 524–531, Feb. 2013.

[10] Genovesi, S., F. Costa, F. Fanciulli, and A. Monorchio, "Wearable inkjet-printed wideband antenna by using miniaturized AMC for sub-GHz applications," *IEEE Antennas and Wireless Propagation Letters*, Vol. 15, 1927–1930, 2016.

[11] Agarwal, K., Y.-X. Guo, and B. Salam, "Wearable AMC backed near-endfire antenna for on-body communications on latex substrate," *IEEE Transactions on Components, Packaging and Manufacturing Technology*, Vol. 6, No. 3, 346–358, Mar. 2016.

[12] Jiang, Z. H., Z. Cui, T. Yue, Y. Zhu, and D. H. Werner, "Compact, highly efficient, and fully flexible circularly polarized antenna enabled by silver nanowires for wireless body-area networks," *IEEE Transactions on Biomedical Circuits and Systems*, Vol. 11, No. 4, 920–932, Aug. 2017.

[13] Yan, S., P. J. Soh, and G. A. E. Vandenbosch, "Low-profile dual-band textile antenna with artificial magnetic conductor plane," *IEEE Transactions on Antennas and Propagation*, Vol. 62, No. 12, 6487–6490, Dec. 2014.

[14] Liu, X., Y. Di, H. Liu, Z. Wu, and M. M. Tentzeris, "A planar windmill-like broadband antenna equipped with artificial magnetic conductor for off-body communications," *IEEE Antennas and Wireless Propagation Letters*, Vol. 15, 64–67, 2016.

[15] Naoui, S., L. Latrach, and A. Gharsallah, "Equivalent circuit model of double split ring resonators," *International Journal of Microwave and Optical Technology*, Vol. 11, No. 1, 1–6, 2016.

[16] Makarov, S. N., G. M. Noetscher, J. Yanamadala, M. W. Piazza, S. Louie, A. Prokop, A. Nazarian, and A. Nummenmaa, "Virtual human models for electromagnetic studies and their applications," *IEEE Reviews in Biomedical Engineering*, Vol. 10, 95–121, 2017.

[17] Kamel, Y. A., H. A. Mohamed, H. ELsadek, and H. El-Hennawy, "Flexible wearable antenna based on AMC with different materials for bio-telemetry applications," *Progress In Electromagnetics Research M*, Vol. 127, 1–10, 2024.

[18] Shah, A. and P. Patel, "Suspended embroidered triangular e-textile broadband antenna loaded with shorting pins," *AEU — International Journal of Electronics and Communications*, Vol. 130, 153573, 2021.

[19] Nie, H.-K., X.-W. Xuan, and G.-J. Ren, "Wearable antenna pressure sensor with electromagnetic bandgap for elderly fall monitoring," *AEU — International Journal of Electronics and Communications*, Vol. 138, 153861, 2021.